Available online at www.sciencedirect.com
SCIENCE DIRECT®
Journal of Solid State Chemistry 177 (2004) 4680–4686
JOURNAL OF SOLID STATE CHEMISTRY
www.elsevier.com/locate/jssc

Two new octahedral/pyramidal frameworks containing both cation channels and lone-pair channels: syntheses and structures of $Ba_2Mn^{II}Mn_2^{III}(SeO_3)_6$ and $PbFe_2(SeO_3)_4$

Magnus G. Johnston, William T.A. Harrison*

Department of Chemistry, University of Aberdeen, Meston Walk, Aberdeen, Scotland AB24 3UE, UK

Received 13 January 2004; received in revised form 18 May 2004; accepted 14 July 2004

Abstract

The hydrothermal syntheses, single crystal structures, and some properties of $Ba_2Mn^{II}Mn_2^{III}(SeO_3)_6$ and $PbFe_2(SeO_3)_4$ are reported. These related phases contain three-dimensional frameworks of vertex (FeO_6) and vertex/edge linked (MnO_6) octahedra and SeO_3 pyramids. In each case, the MO_6/SeO_3 framework encloses two types of 8 ring channels, one of which encapsulates the extra-framework cations and one of which provides space for the Se^{IV} lone pairs. Crystal data: $Ba_2Mn_3(SeO_3)_6$, $M_r = 1201.22$, monoclinic, $P2_1/c$ (No. 14), $a = 5.4717$ (3) Å, $b = 9.0636$ (4) Å, $c = 17.6586$ (9) Å, $\beta = 94.519$ (1)°, $V = 873.03$ (8) Å^3, $Z = 2$, $R(F) = 0.031$, $wR(F^2) = 0.070$; $PbFe_2(SeO_3)_4$, $M_r = 826.73$, triclinic, $P\bar{1}$ (No. 2), $a = 5.2318$ (5) Å, $b = 6.7925$ (6) Å, $c = 7.6445$ (7) Å, $\alpha = 94.300$ (2)°, $\beta = 90.613$ (2)°, $\gamma = 95.224$ (2)°, $V = 269.73$ (4) Å^3, $Z = 1$, $R(F) = 0.051$, $wR(F^2) = 0.131$.

Keywords: Hydrothermal synthesis; Crystal structures; Selenites

1. Introduction

The structures of extended inorganic networks incorporating the $[SeO_3]^{2-}$ selenite ion are of interest due to the asymmetric coordination polyhedron adopted by this species, as described in the extensive, recent review of Verma [1]. The effect can be rationalized in terms of the stereochemically active lone pair of electrons associated with Se^{IV}, which are always directed away from the three O atoms, as predicted by VSEPR theory [2], leading to pyramidal coordination for the selenite species. It has been suggested that this inherently asymmetric geometry for Se^{IV} may lead to a tendency for selenites to crystallize in noncentrosymmetric structures with consequent interesting physical properties [3], such as second harmonic generation (SHG).

In this paper, we report the hydrothermal syntheses, single-crystal structures, and some properties of $Ba_2Mn^{II}Mn_2^{III}(SeO_3)_6$ and $PbFe_2(SeO_3)_4$. These related phases demonstrate a self-containment effect [4] in which the Se^{IV} lone pairs of electrons are directed into otherwise empty, infinite, one-dimensional 8-ring channels of significant size. A similar effect has recently been demonstrated for the phase $Tb_2O(SeO_3)_2$, in which the selenite moieties arrange themselves so that their lone pairs occupy channels in a manner that reflects the $\bar{4}$ symmetry of other parts of the structure [5].

2. Experimental

Syntheses: $Ba_2Mn_3(SeO_3)_6$ was prepared by a hydrothermal reaction, as follows: 0.395 g (2 mmol) $BaCO_3$, 0.209 g (1 mmol) $MnCl_2 \cdot 4H_2O$, 0.536 g (2 mmol) $Mn(CH_3CO_2)_3 \cdot 2H_2O$, 0.666 g (6 mmol) SeO_2 and 15 ml H_2O were sealed in a 23 ml capacity, teflon-lined

*Corresponding author. Fax: +44-1224-272-921.
E-mail address: w.harrison@abdn.ac.uk (W.T.A. Harrison).

0022-4596/$ - see front matter © 2004 Elsevier Inc. All rights reserved.
doi:10.1016/j.jssc.2004.07.057

stainless steel bomb. The bomb was heated to 140 °C for 4 days, followed by cooling to room temperature over a few hours. The solid product, consisting of a mass of brown rods and needles, was recovered from the supernatant liquors by vacuum filtration and washing with water and acetone. Powder XRD (see below) indicated the presence of a small (visual estimate, based on peak heights, of perhaps 2%) quantity of $Mn^{II}Mn^{III}_2O(SeO_3)_3$. This phase [6] also crystallizes as brown needles, making phase separation extremely difficult.

$PbFe_2(SeO_3)_4$ initially arose from a very surprising reaction: 2 g $MgSO_4 \cdot 7H_2O$ (BDH Analar), 5 g SeO_2 (Lancaster Synthesis), and 15 ml deionised H_2O were sealed in a 23 ml hydrothermal bomb and heated to 200 °C for two days, followed by cooling to room temperature over a few hours. The solid product, consisting of a tiny yield (<1 mg) of yellow–green, faceted, chunks of $PbFe_2(SeO_3)_4$ was recovered by vacuum filtration and washing with water and acetone. This reaction is reproducible. No lead or iron compounds had been recently prepared using the hydrothermal bomb in question; thus, presumably, impurities in the starting material(s) reacted to form the $PbFe_2(SeO_3)_4$ product. This is supported by trace-elemental analysis results: the Lancaster SeO_2 sample contained 4.24 (9) μg/kg Pb whereas the lead content of the magnesium nitrate heptahydrate was negligible (below detection limits). The iron probably arose from the Analar $MgSO_4 \cdot 7H_2O$ [Fe content = 9.37 (11) μg/kg] whereas the Lancaster SeO_2 contained negligible Fe (at or below detection limits).

EDX indicated the presence of Pb, Fe, and Se in the crystalline chunks, which was confirmed in the crystal-structure study described below. A rational hydrothermal synthesis started from 0.662 g (2 mmol) $Pb(NO_3)_2$, 1.616 g (4 mmol) $Fe(NO_3)_3 \cdot 9H_2O$, 0.888 g (8 mmol) SeO_2 (BDH Analar with negligible Pb content as determined by trace element analysis) and 15 ml H_2O, which were sealed in a 23-ml bomb and heated to 200 °C for 2 days, followed by cooling to room temperature over a few hours. Product recovery as above led to a mixture of tiny (<0.02 mm) yellow cuboids of $PbFe_2(SeO_3)_4$ accompanied by brown whiskers and needles of $Fe_2O(SeO_3)_4$ [7] (identified on the basis of its unit cell parameters), in about a 50:50 ratio (visual estimate).

2.1. Characterization

Powder XRD (Bruker D8 diffractometer, Cu$K\alpha$ radiation, $\lambda = 1.5418$ Å, $T = 20°$ C) on a well-ground sample of $Ba_2Mn_3(SeO_3)_6$ yielded a pattern in good agreement with a simulation based on the single crystal structure accompanied by a few weak lines corresponding to $Mn_3O(SeO_3)_3$ [6]. TGA (Mettler Toledo Star system; ramp at 10 °C/min under argon) for $Ba_2Mn_3(SeO_3)_6$ showed two distinct weight losses (–39.8% occurring between 350 and 700 °C and –14.4% between 800 and 1200 °C). The overall weight loss of 54.2% correlates reasonably well with that calculated (55.4%) for the decomposition scheme $Ba_2Mn_3(SeO_3)_6$ (s) → $Ba_2Mn_3O_6$ (s) + 6 SeO_2 (g), allowing for the presence of a small quantity of $Mn_3O(SeO_3)_3$. The identity of the intermediate decomposition stage at 700 °C is not known. There was insufficient amount of pure sample of $PbFe_2(SeO_3)_4$ to perform similar measurements. The temperature ranges for the decomposition steps reported here for $Ba_2Mn_3(SeO_3)_6$ are wide (up to 400 °C), but similar sluggish decompositions have been seen for other selenites [1].

The diffuse reflectance spectrum (reference standard $BaSO_4$) of $Ba_2Mn_3(SeO_3)_6$ was recorded on a Shimadzu UV-3100 spectrometer at room temperature and converted according to the Kubelka Munk method. It shows a broad, relatively weak absorbance ($\varepsilon \approx 5$) centered at about 500 nm (20,000 cm^{-1}), which probably corresponds to a nominal $^5E_g \rightarrow {}^5T_{2g}$ transition [8] for Mn^{3+} (i.e., promotion of an electron from a t_{2g}-like state to an e_g-like state assuming approximate octahedral symmetry). Any spin-forbidden *d–d* transitions associated with Mn^{2+} are expected to be up to two orders of magnitude weaker [8].

2.2. Structure determinations

The structures of $Ba_2Mn_3(SeO_3)_6$ (brown rod, $\sim 0.04 \times 0.04 \times 0.37$ mm^3) and $PbFe_2(SeO_3)_4$ (yellow–green chunk, $\sim 0.082 \times 0.045 \times 0.045$ mm^3) were determined by standard X-ray methods using data collected on a Bruker SMART CCD diffractometer (Mo$K\alpha$ radiation, $\lambda = 0.71073$ Å, $T = 25 \pm 2$ °C). In each case, a hemisphere of data was collected using ω scans (0.3° slices) with the aid of the SMART and SAINT programs [9], and empirical absorption corrections (min./max. transmission coefficients = 0.053/0.515 and 0.181/0.329 for $Ba_2Mn_3(SeO_3)_6$ and $PbFe_2(SeO_3)_4$, respectively) was made with SADABS [10] during data reduction. The systematic absences for $Ba_2Mn_3(SeO_3)_6$ indicated space group $P2_1/c$ (No. 14) which was assumed for the remainder of the refinement. For $PbFe_2(SeO_3)_4$, the situation is somewhat less clear cut. Structure solution and refinement in space group $P\bar{1}$ (No. 2) resulted (see below) in a generally satisfactory answer, except for excessively large anisotropy of the lead atom displacement parameters [$U_{max}/U_{min} = 7.7$]. Thus, a model involving positional disorder of the Pb species over two adjacent sites related by inversion symmetry was developed [refined $d(Pb\cdots Pb^i) = 0.449$ (3) Å; symmetry code (i) = $-x$, $-y$, $-z$; $U_{max}/U_{min} = 2.9$]. A refinement was also performed in space group $P1$ (No. 1), but this also led to disorder over two adjacent, nonsymmetry-related sites [$d(Pb\cdots Pb) = 0.495$ (5) Å] and

Table 1
Crystallographic parameters

	$Ba_2Mn_3(SeO_3)_6$	$PbFe_2(SeO_3)_4$
Empirical formula	$Ba_2Se_6Mn_3O_{18}$	$PbSe_4Fe_2O_{12}$
Formula weight	1201.26	826.73
Crystal system	Monoclinic	Triclinic
Crystal color, form	Brown rod	Yellow–green chunk
a (Å)	5.4717 (3)	5.2318 (5)
b (Å)	9.0636 (4)	6.7925 (6)
c (Å)	17.6586 (9)	7.6445 (7)
α (°)	90	94.300 (2)
β (°)	94.519 (1)	90.613 (2)
γ (°)	90	95.224 (2)
V(Å^3)	873.03 (8)	269.73 (4)
Z	2	1
Space group	$P2_1/c$ (No. 14)	$P\bar{1}$(No. 2)
T (°C)	20±2	20±2
λ (Mo$K\alpha$) (Å)	0.71073	0.71073
ρ_{calc} (g/cm^3)	4.57	5.09
μ (cm^{-1})	191.5	317.8
Maximum 2θ (°)	65.0	65.0
Reflections measured	6923	2800
R_{int}	0.034	0.027
Merged/observed[a] reflections	3149/2657	1874/1443
Parameters	133	94
Coverage of unique data (%)	99.6	96.2
$R(F)$[b]	0.031	0.051
$wR(F^2)$[c]	0.070	0.131

[a] $I > 2\sigma(I)$ after the merging of systematically equivalent and multiply measured reflections.
[b] $R = \Sigma\big||F_o| - |F_c|\big| / \Sigma|F_o|$ for merged data with $I > 2\sigma(I)$.
[c] $wR = [\Sigma w(|F_o^2| - |F_c^2|)^2 / \Sigma w|F_o^2|^2]^{1/2}$ for all merged data.

essentially the same residuals, and was discarded. For both structures, direct methods using SHELXS-97 [11] were used to locate most of the atoms, and the remaining atoms were located from difference maps during the full-matrix least-squares refinements using SHELXL-97 [11]. Neither structure required charge balancing by protons. Crystallographic data are summarized in Table 1. Supplementary materials are available from the authors by e-mail or from the Fachinformationzentrum (FIZ), Karlsruhe, Germany [deposition numbers CSD-414051 for $Ba_2Mn_3(SeO_3)_6$ and CSD-414053 for $PbFe_2(SeO_3)_4$].

3. Results

3.1. Crystal structure of $Ba_2Mn_3(SeO_3)_6$

Atomic coordinates and displacement parameters and selected geometrical data are presented in Tables 2 and 3, respectively. This phase contains 15 atoms (1 Ba, 2 Mn, 3 Se, 9 O) in the asymmetric unit (Fig. 1), all of which occupy general positions, except Mn1 (site symmetry $\bar{1}$). Both manganese cations have six neighboring O atoms; the Mn1 grouping [d_{av}(Mn1–O) = 2.194 (3) Å] is essentially a regular octahedron, whereas the Mn2 coordination [d_{av}(Mn2–O) = 2.043 (3) Å] is substantially distorted from octahedral regularity, and could also be described as an elongated tetragonal bipyramid, although the axial O–Mn–O bond angle of 146.61 (12)° is far removed from the nominal value of 180°. The Mn2 polyhedron can be quantified in terms of the distance distortion [12] $\Delta_{oct} = 0.0068$ and the angular variance [13] $\sigma^2_{oct} = 116.5$. Bond valence sum (BVS) calculations, using the Brown [14] formalism, yield BVS(Mn1) = 2.01, and BVS(Mn2) = 3.06, strongly suggesting that Mn1 is divalent and Mn2 is trivalent. This presence of mixed-valence Mn^{2+}/Mn^{3+} is also consistent with the brown crystal color [15] and the diffuse reflectance spectrum of $Ba_2Mn_3(SeO_3)_6$ (see above). The distortion of the $Mn2O_6$ octahedron can be explained by the Jahn–Teller effect for d^4 Mn^{III}, and the average Mn–O distance seen here is in excellent agreement with the relationship $\bar{d}(Mn^{III}–O) = (1.994 + 7.08\ \Delta_{oct}) = 2.042$ Å established by Shannon et al. [12] for other trivalent manganese compounds. The three selenium atoms show their normal coordination behavior [1,16] of three O atom neighbors in pyramidal conformation [d_{av}(Se–O) = 1.704 (3) Å], with the fourth tetrahedral vertex assumed to be occupied by the Se^{IV} lone pair of electrons. O2 and O3 form a common edge between the Mn2 and Se1 groups, and the other O atoms form vertex-sharing Mn–O–Se bridges ($\theta_{av} = 129.5°$). All but O7 and O8 also bond to the barium cation which could be described as either nine or [if the longer Ba1–O1 bond of 3.318(3) Å is included] ten coordinate [spread of Ba–O distances = 2.729(3)–3.012(2) + 3.318(3) Å; mean for 9 values = 2.820 Å; mean for 10 values = 2.869 Å] and the Ba^{2+} bond valence sum [14] is 2.24 (expected 2.00) indicating that its valence requirements are satisfied in this structure.

Table 2
Atomic coordinates/displacement parameters for $Ba_2Mn_3(SeO_3)_6$

Atom	x	y	z	U_{eq}
Ba1	−0.01925(4)	0.33191(3)	0.203911(14)	0.01187(6)
Mn1	0	$\frac{1}{2}$	0	0.01221(16)
Mn2	0.51495(11)	−0.00133(7)	0.16398(4)	0.01130(12)
Se1	0.50497(7)	0.14602(4)	0.31342(2)	0.01082(8)
Se2	0.49958(7)	0.29574(5)	0.04648(2)	0.01157(9)
Se3	0.00833(7)	0.86033(5)	0.06694(2)	0.01273(9)
O1	0.5531(5)	0.3240(3)	0.28145(18)	0.0153(6)
O2	0.2623(5)	0.0960(3)	0.25312(18)	0.0148(6)
O3	0.7189(5)	0.0664(3)	0.26060(16)	0.0132(5)
O4	0.2375(5)	0.3623(4)	0.07730(19)	0.0185(6)
O5	0.6036(6)	0.1812(4)	0.1205(2)	0.0208(7)
O6	0.7026(5)	0.4324(3)	0.06780(17)	0.0148(6)
O7	0.0884(6)	0.6833(4)	0.0792(2)	0.0216(7)
O8	0.2825(6)	0.9554(4)	0.08245(19)	0.0233(7)
O9	−0.1398(6)	0.8942(4)	0.14531(18)	0.0219(7)

Table 3
Selected bond lengths (Å) and angles (°) for $Ba_2Mn_3(SeO_3)_6$

Ba1–O3^{i}	2.729 (3)
Ba1–O2	2.737 (3)
Ba1–O4	2.747 (3)
Ba1–O9^{ii}	2.793 (3)
Ba1–O5^{iii}	2.796 (3)
Ba1–O1^{iii}	2.804 (3)
Ba1–O2^{iv}	2.869 (3)
Ba1–O6^{iii}	2.889 (3)
Ba1–O3^{iii}	3.012 (3)
Ba1–O1	3.318 (3)
Mn1–O6^{v}	2.183 (3)
Mn1–O6^{iii}	2.183 (3)
Mn1–O4	2.198 (3)
Mn1–O4^{vi}	2.198 (3)
Mn1–O7^{vi}	2.201 (3)
Mn1–O7	2.201 (3)
Mn2–O8^{vii}	1.886 (3)
Mn2–O5	1.903 (3)
Mn2–O1^{viii}	1.905 (3)
Mn2–O3	2.057 (3)
Mn2–O9^{ix}	2.161 (3)
Mn2–O2	2.347 (3)
Se1–O2	1.697 (3)
Se1–O3	1.713 (3)
Se1–O1	1.736 (3)
Se2–O4	1.685 (3)
Se2–O6	1.686 (3)
Se2–O5	1.730 (3)
Se3–O7	1.673 (3)
Se3–O9	1.686 (3)
Se3–O8	1.733 (3)
Se1–O1–Mn2^{i}	124.54 (17)
Se1–O2–Mn2	92.75 (12)
Se1–O3–Mn2	103.18 (13)
Se2–O4–Mn1	118.64 (17)
Se2–O5–Mn2	138.39 (19)
Se2–O6–Mn1^{x}	126.17 (16)
Se3–O7–Mn1	126.82 (19)
Se3–O8–Mn2^{xi}	138.37 (19)
Se3–O9–Mn2^{xii}	133.43 (19)

Symmetry transformations used to generate equivalent atoms: (i) $1-x$, $y+1/2$, $1/2-z$; (ii) $-x$, $y-1/2$, $1/2-z$; (iii) $x-1$, y, z; (iv) $-x$, $y+1/2$, $1/2-z$; (v) $1-x$, $1-y$, $-z$; (vi) $-x$, $1-y$, $-z$; (vii) x, $y-1$, z; (viii) $1-x$, $y-1/2$, $1/2-z$; (ix) $x+1$, $y-1$, z; (x) $x+1$, y, z; (xi) x, $y+1$, z; (xii) $x-1$, $y+1$, z.

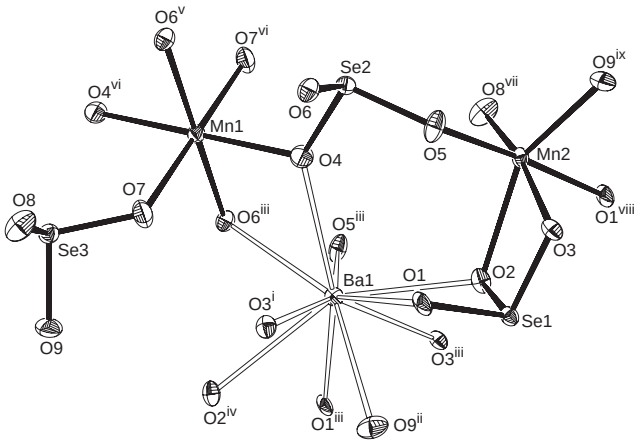

Fig. 1. Fragment of $Ba_2Mn_3(SeO_3)_6$, showing the atomic connectivity (50% displacement ellipsoids). Symmetry codes as in Table 3.

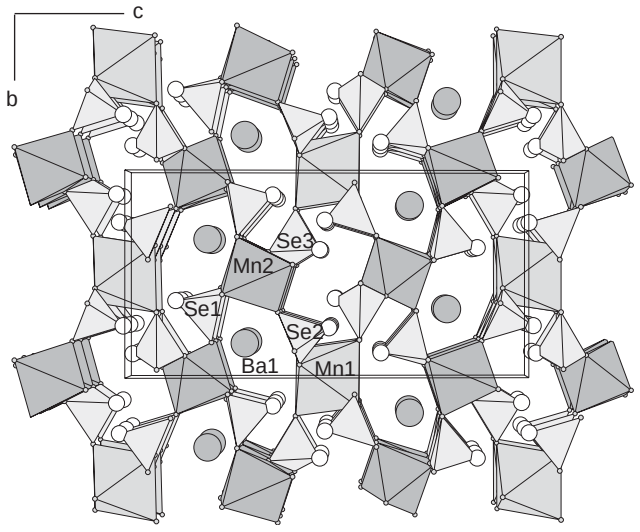

Fig. 2. Polyhedral view projected onto (1 0 0) for $Ba_2Mn_3(SeO_3)_6$ showing the network of $Mn1O_6$, $Mn2O_6$ octahedra (light and dark shading, respectively) and SeO_3E pseudo tetrahedra [the dummy atom E (unshaded circle), placed 1.0 Å from Se represents the lone pair of electrons] encapsulating channels at $y \approx 0.33$, $z \approx 0.20$ and equivalent locations occupied by the barium cations (shaded circles) and Se1 lone pairs and empty lone-pair channels at $y = 0$, $z = 0$ and equivalent locations occupied by the Se2 and Se3 lone pairs.

The polyhedral connectivity (Fig. 2) in $Ba_2Mn_3(SeO_3)_6$ can be described as follows: twisted chains of $Mn2O_6$ (trivalent Mn) and $Se1O_3$ groups, alternately sharing edges (via O2 + O3) and vertices (via O1), propagate along [010]. The edge-sharing Mn–O–Se bond angles are much smaller than the vertex-sharing Mn–O–Se angles and also correlate with the very compressed O2–Mn2–O3 octahedral [68.99 (10)°] and O2–Se1–O3 [94.60 (14)°] pyramidal bond angles. The $Mn1O_6$ and $Se2O_3$ groups form 4-ring (four polyhedral units) chains by vertex sharing and propagate along [1 0 0], with the manganese atoms serving to fuse the links of the chain. Thus, each Mn1 atom is bonded to four distinct Se2 species. Pairs of $Se3O_3$ groups are also attached to the Mn1 centers in *trans* configuration. Cross linking between the Mn1/Se2/Se3 and Mn2/Se1 chains by way of both the $Se2O_3$ and $Se3O_3$ groups results in a three-dimensional, anionic, framework in which the Mn- and Se-centered polyhedra strictly alternate. The $[Mn_3(SeO_3)_6]^{2-}$ framework contains two types of channels propagating along [100], both comprised of eight polyhedral units (8 rings) alternating between MnO_6 and SeO_3. The first of these (atom-to-atom dimensions $\sim 3.40 \times 6.18$ Å) is occupied by the Ba^{2+} species. In addition, the Se1 lone pair appears to point into this channel. The second channel provides

space for the Se2 and Se3 lone pairs and is empty of any other chemical species, despite its atom-to-atom dimensions of some 3.99×5.42 Å.

3.2. Crystal structure of $PbFe_2(SeO_3)_4$

This phase contains 12 atoms (2 Pb, 2 Fe, 2 Se, 6 O) in the asymmetric unit (Fig. 3), with the lead species statistically disordered over two adjacent sites (see above) and both iron cations occupying inversion centers. Atomic positional and displacement parameters are listed in Table 4 and selected geometrical data are shown in Table 5. Both iron cations have essentially regular octahedral coordination [d_{av}(Fe1–O) = 2.002 (7) Å and d_{av}(Fe2–O) = 2.035 (7) Å] and bond valence sum calculations [14] [BVS(Fe1) = 3.11, BVS(Fe2) = 2.88] confirm the presence of trivalent iron. The two distinct pyramidal selenite groups have typical geometrical parameters [d_{av}(Se1–O) = 1.707 (7) Å, BVS(Se1) = 3.98; d_{av}(Se2–O) = 1.706 (7) Å, BVS(Se2) = 3.99]. The six O atoms all form Fe–O–Se bridges ($\theta_{av} = 126.2^\circ$), thus there is no edge-sharing in this phase, and all but O1 and O3 also bond to the lead cation (Table 5).

The Pb^{2+} species in $PbFe_2(SeO_3)_4$ can be described as 4 + 5 coordinate; with four O atom near neighbors [d(Pb–O) < 2.6 Å] arranged in approximately square planar conformation, with five more distant atoms [d(Pb–O) > 2.9 Å] completing an irregular coordination with a large spread of distances of 0.714 Å. The BVS [14] for Pb1 of 1.66 (expected = 2.00) for the nine nearest O atoms suggests a significant degree of underbonding which may correlate with the space-filling requirements of the Pb^{2+} lone pair, although it is difficult to visualize in which direction this may point. The next-nearest O atom is over 3.5 Å from the lead atom.

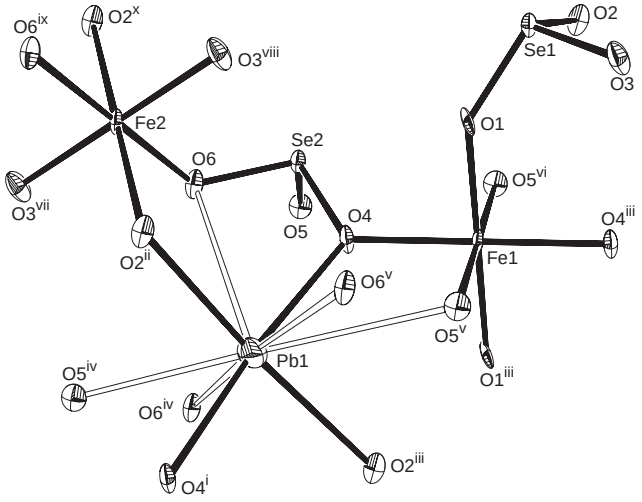

Fig. 3. Fragment of $PbFe_2(SeO_3)_4$, showing the atomic connectivity (50% displacement ellipsoids). Symmetry codes as in Table 5. The longer (d > 2.75 Å) Pb–O bonds are shown as open lines.

Table 4
Atomic coordinates/displacement parameters for $PbFe_2(SeO_3)_4$

Atom	x	y	z	U_{eq}
Pb1[a]	0.0387(4)	−0.0059(5)	−0.0105(4)	0.0254(4)
Fe1	0	0	$\frac{1}{2}$	0.0092(3)
Fe2	$\frac{1}{2}$	$\frac{1}{2}$	0	0.0096(3)
Se1	−0.00877(13)	0.45083(11)	0.74140(10)	0.00929(17)
Se2	0.51726(13)	0.19967(11)	0.32356(10)	0.00960(18)
O1	0.0138(11)	0.2906(9)	0.5642(7)	0.0131(11)
O2	0.1531(10)	0.3480(9)	0.9065(8)	0.0136(11)
O3	−0.3227(11)	0.4001(10)	0.7904(8)	0.0182(12)
O4	0.2212(10)	0.0695(9)	0.2951(7)	0.0127(11)
O5	0.7052(10)	0.0111(9)	0.3341(8)	0.0141(11)
O6	0.5731(10)	0.2455(9)	0.1094(8)	0.0141(11)

[a]Site occupancy for Pb1 = $\frac{1}{2}$.

Table 5
Selected bond lengths (Å) and angles (°) for $PbFe_2(SeO_3)_4$

Pb1–O4	2.513 (7)
Pb1–O4^{i}	2.541 (6)
Pb1–O2^{ii}	2.552 (6)
Pb1–O2^{iii}	2.629 (6)
Pb1–O6^{iv}	2.792 (6)
Pb1–O5^{iv}	2.825 (6)
Pb1–O5^{v}	3.176 (6)
Pb1–O6^{v}	3.203 (6)
Pb1–O6	3.227 (6)
Fe1–O1^{iii}	1.993 (6)
Fe1–O1	1.993 (6)
Fe1–O5^{vi}	1.997 (6)
Fe1–O5^{v}	1.997 (6)
Fe1–O4^{iii}	2.016 (5)
Fe1–O4	2.016 (5)
Fe2–O3^{vii}	1.968 (6)
Fe2–O3^{viii}	1.968 (6)
Fe2–O6	2.041 (6)
Fe2–O6^{ix}	2.041 (6)
Fe2–O2^{x}	2.095 (5)
Fe2–O2^{ii}	2.095 (5)
Se1–O1	1.685 (6)
Se1–O3	1.699 (6)
Se1–O2	1.736 (6)
Se2–O5	1.690 (6)
Se2–O6	1.712 (6)
Se2–O4	1.716 (5)
Se1–O1–Fe1	140.1 (3)
Se1–O2–Fe2^{xi}	117.2 (3)
Se1–O3–Fe2^{xii}	127.1 (4)
Se2–O4–Fe1	121.9 (3)
Se2–O5–Fe1^{xiii}	126.5 (3)
Se2–O6–Fe2	124.7 (3)

Symmetry transformations used to generate equivalent atoms: (i) $-x$, $-y$, $-z$; (ii) x, y, $z-1$; (iii) $-x$, $-y$, $1-z$; (iv) $1-x$, $-y$, $-z$; (v) $x-1$, y, z; (vi) $1-x$, $-y$, $1-z$; (vii) $x+1$, y, $z-1$; (viii) $-x$, $1-y$, $1-z$; (ix) $1-x$, $1-y$, $-z$; (x) $1-x$, $1-y$, $1-z$; (xi) x, y, $z+1$; (xii) $x-1$, y, $z+1$; (xiii) $x+1$, y, z.

The polyhedral connectivity (Fig. 4) in $PbFe_2(SeO_3)_4$ consists of chains of the Fe1, Se1 and Se2-centered moieties propagating along [100]. Each Fe1 center is

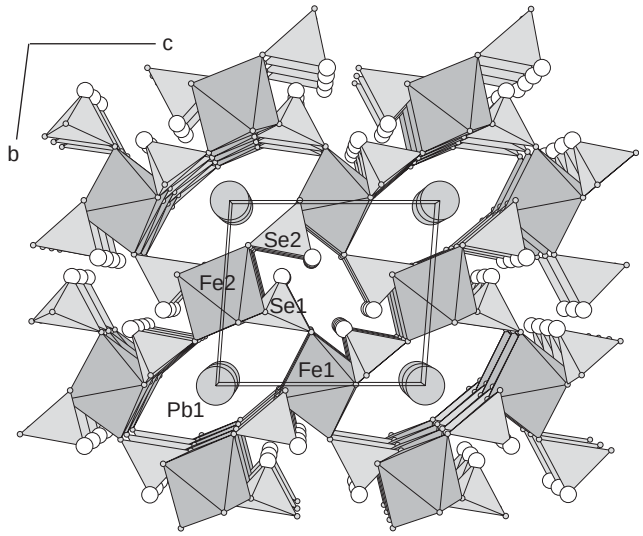

Fig. 4. Polyhedral view projected onto (1 0 0) for $PbFe_2(SeO_3)_4$ showing the network of FeO_6 octahedra and SeO_3E pseudotetrahedra [the dummy atom E (unshaded circle), placed 1.0 Å from Se represents the lone pair of electrons] encapsulating channels at $y=0$, $z=0$ and equivalent locations occupied by the lead cations (shaded circles) and empty lone-pair channels at $y=\frac{1}{2}$, $z=\frac{1}{2}$ and equivalent locations.

bridged to two Fe1 neighbors by way of a pair of $Se2O_3$ groups. The two remaining Fe1 vertices are linked to $Se1O_3$ groups. Crosslinking of the chains by the Fe2 groups results in a three-dimensional FeO_6/SeO_3 network encapsulating two types of channels propagating along [1 0 0]. The first of these at ($y=0$, $z=0$) and equivalent locations, with maximum atom-to-atom dimensions of 3.63×7.99 Å contains the lead cations and the second at ($y=1/2$, $z=1/2$; dimensions = 3.10×6.76 Å), is empty, apart from the unobserved Se lone pairs of electrons.

4. Discussion

The new mixed-metal selenites $Ba_2Mn_3(SeO_3)_6$ and $PbFe_2(SeO_3)_4$ have been hydrothermally prepared as single crystals and characterized. To the best of our knowledge, they are the first well-characterized binary M/M'/selenites to contain these cation combinations. A very puzzling "impurity + impurity reaction" initially prepared the lead phase, which could then be followed up by a more rational synthesis from the appropriate starting materials once the composition and structure were known. However, neither material could be made in entirely pure form by the methods tried here. Both structures consist of three-dimensional octahedral (MnO_6, FeO_6)/pyramidal (SeO_3) networks encapsulating one-dimensional channels which are occupied by the large, divalent cations. The shapes of the manganese, iron and selenium polyhedra can be rationalized in terms of the oxidation states of the species in question, and in the case of $Ba_2Mn_3(SeO_3)_6$, the presence of edge-sharing between the polyhedral units. The irregular nine- or ten-fold coordination of Ba^{2+} in $Ba_2Mn_3(SeO_3)_6$ is typical whereas the nine-fold coordinated Pb^{2+} species in $PbFe_2(SeO_3)_4$ appears to be somewhat under-bonded, perhaps due to its lone-pair stereochemical activity [17]. These species are accommodated in infinite channels, each surrounded by 8 polyhedral building blocks. In both cases, a second one-dimensional channel of significant size exists which is empty of other chemical species. Based on geometrical placement, the Se lone pairs are directed into these 8-ring channels. Unlike the case of $Tb_2O(SeO_3)_2$ [5] there is no obvious symmetry relationship between the packing of the metal-centered octahedra and the Se lone pairs.

$Ba_2Mn_3(SeO_3)_6$ complements various other mixed-valence manganese selenites prepared hydrothermally including $Mn^{II}Mn_2^{III}O(SeO_3)_2$ [6], $KMn_4^{II}Mn^{III}(SeO_3)_6$ [18], and $Li_5Mn_4^{II}Mn^{III}(SeO_3)_8$ [18]. The average Mn–O separations in $Mn^{II}Mn_2^{III}O(SeO_3)_2$ (Mn^{II}–O $d_{av}=2.192$ Å; Mn^{III}–O $d_{av}=2.036$ Å) are very similar to those reported above for $Ba_2Mn_3(SeO_3)_6$ although the overall structures of the two materials are quite different. The essentially regular Mn^{II} coordination in $Ba_2Mn_3(SeO_3)_6$ is completely different to the highly distorted, effectively irregular, manganese(II) environment in $SrMn(SeO_3)_2$ in which edge-sharing occurs between the $Mn^{II}O_6$ and SeO_3 moieties [19]. The recently described [20] manganese selenites $Mn_3(SeO_3)_3\cdot H_2O$ and $Mn_4(SeO_3)_4\cdot 3H_2O$ also possess very distorted MnO_6 groupings.

The occurrence of lone-pair channels of reasonable size and redox-active Mn^{II}/Mn^{III} metal centers in $Ba_2Mn_3(SeO_3)_6$ suggests the possibility of redox intercalation in which a process schematically represented by $Ba_2Mn^{II}Mn_2^{III}(SeO_3)_6+Li\rightarrow Li_xBa_2Mn^{II}_{1+x}Mn^{III}_{2-x}(SeO_3)_6$ ($0\leqslant x\leqslant 2$) could occur and we are now investigating this possibility further.

Acknowledgments

We thank Brian Paterson for assistance with the TGA measurement. We thank Andrea Raab and Jörg Feldmann (Trace Element Speciation Laboratory Aberdeen) for their invaluable assistance with the elemental analysis. We thank an anonymous referee for helpful crystallographic suggestions.

References

[1] V.P. Verma, Thermochim. Acta 327 (1999) 63.
[2] J.K. Burdett, Molecular Shapes, Wiley-Interscience, New York, 1980.
[3] K.M. Ok, P.S. Halasyamani, Chem. Mater. 14 (2002) 2360.

[4] M.G. Johnston, W.T.A. Harrison, J. Am. Chem. Soc. 124 (2002) 4576.
[5] J. Wontcheu, T. Schleid, Zeit. Anorg. Allg. Chem. 628 (2002) 1941.
[6] M. Wildner, J. Solid State Chem. 113 (1994) 252.
[7] G. Giester, Zeit. Kristallogr. 211 (1996) 603.
[8] A.B.P. Lever, Inorganic Electron Spectroscopy, Elsevier, Amsterdam, 1984, p. 434.
[9] Software for SMART diffractometers, Bruker AXS Inc., Madison, WI, USA.
[10] G.M. Sheldrick, Program SADABS for Absorption Corrections for Area-detector Data, University of Göttingen, Germany, 1999.
[11] G.M. Sheldrick, Programs SHELXS-97 and SHELXL-97 for Solving and Refining Single Crystal Data, University of Göttingen, Germany, 1997.
[12] R.D. Shannon, P.S. Gumerman, J. Chenavas, Am. Miner. 60 (1975) 714.
[13] K. Robinson, G.V. Gibbs, P.H. Ribbe, Science (Washington, DC) 172 (1971) 567.
[14] I.D. Brown, J. Appl. Crystallogr. 29 (1996) 479.
[15] K.F. Hsu, S.L. Wang, Chem. Commun. (2000) 135.
[16] M. Wildner, Monatsch. Chem. 122 (1991) 585.
[17] E. Morin, G. Wallez, S. Jaulmes, J.C. Couturier, M. Quarton, J. Solid State Chem. 137 (1998) 283.
[18] M. Wildner, J. Solid State Chem. 103 (1993) 341.
[19] M.G. Johnston, W.T.A. Harrison, Acta Crystallogr. C 58 (2002) i33.
[20] A. Larrahaga, J.L. Mesa, J.L. Pizarro, M.I. Olazcuaga. T. Rojo, J. Chem. Soc. Dalton Trans. (2002) 2447.